Applied Catalysis B: Environmental 220 (2018) 615–625

Contents lists available at ScienceDirect

Applied Catalysis B: Environmental

journal homepage: www.elsevier.com/locate/apcatb

Research Paper

CO_2 methanation on Ru/TiO_2 catalysts: On the effect of mixing anatase and rutile TiO_2 supports

Ara Kim[a,b], Damien P. Debecker[a,*], François Devred[a], Vincent Dubois[c], Clément Sanchez[b], Capucine Sassoye[b,*]

[a] Institute of Condensed Matter and Nanosciences – Molecules, Solids and Reactivity (IMCN – MOST), Université catholique de Louvain, Place Louis Pasteur, 1, box L4. 01.09, 1348 Louvain-La-Neuve, Belgium

[b] Sorbonne Universités, UPMC Université Paris, CNRS, Collège de France, Laboratoire de Chimie de la Matière Condensée de Paris, 4 Place Jussieu, 75252 Paris Cedex, France

[c] Institut Meurice, Laboratoire de Chimie Physique et Catalyse,Avenue Emile Gryson, 1–B-1070 Brussels, Belgium

ARTICLE INFO

Keywords:
CO_2 hydrogenation
RuO_2 nanoparticles
Titania
Epitaxy
Sabatier reaction

ABSTRACT

The high CO_2 methanation activity of Ru/TiO_2 catalysts prepared by mixing both anatase and rutile TiO_2 as a support is described, focusing on mild reaction temperature (50–200 °C). The specific catalyst design elucidated the impact of the support mixing. Pre-synthesized, monodispersed 2 nm-RuO_2 nanoparticles were used to serve as precursors for active metallic Ru responsible for the CO_2 hydrogenation reaction. Pure TiO_2 supports with different crystallinity (anatase and rutile) were either prepared in the laboratory or obtained from commercial providers, mixed, and used as supports in different ratios. The mixing was also done at different stages of the catalyst preparation, i.e. before RuO_2 deposition, before annealing or after annealing. Our study uncovers that the interaction between the RuO_2 nanoparticles and the anatase and rutile TiO_2 phase during the annealing step dictates the performance of the Ru/TiO_2 methanation catalysts. In particular, when beneficial effects of support mixing are obtained, they can be correlated with RuO_2 migration and stabilization over rutile TiO_2 through epitaxial lattice matching. Also, support mixing can help prevent the sintering of the support and the trapping of the active phase in the bulk of the sintered support. On thermally stable TiO_2 supports, however, it appears clearly that the sole presence of rutile TiO_2 support is sufficient to stabilize Ru in its most active form and to prepare a catalyst with high specific activity.

1. Introduction

In recent years, there has been increasing pressure in the society to curb CO_2 emissions and develop efficient CO_2 capture, storage and utilization technologies [1–4]. The reduction of CO_2 emissions is recognized as a long term task as it requires efficient use of energy and switching from fossil fuels towards less carbon intensive energy sources such as hydrogen and renewable energy [4,5]. In regard to the reduction of CO_2 in the atmosphere, two major strategies have been proposed: CO_2 capture and storage, or usage of CO_2 [4,6–12]. The usage of CO_2 is particularly promising as increasing amounts of low-cost and relatively pure CO_2 from current and scheduled plants for carbon capture and storage will be available at nearly zero cost [13].

Among different catalytic conversion processes of CO_2, the hydrogenation of CO_2 to methane, so-called CO_2 methanation, is attractive: the reaction can be carried out under atmospheric pressure, the produced CH_4 can be directly injected into already existing natural gas pipelines, and it can be used as a fuel or raw material for production of other chemicals [10]. Thus, CO_2 methanation can serve as a tool for H_2 produced from renewable resources to be efficiently utilized as an energy vector since transportation of H_2 is limited due to its low volumetric energy density [14].

CO_2 methanation via heterogeneous catalysts has received considerable attention in recent years [3,10,15]. Numerous supported metals, such as Ni, Ru, Rh, Pd, Co, and Mg on various oxide supports, including TiO_2, SiO_2, Al_2O_3, CeO_2, MgO and ZrO_2, have been investigated [16–23]. The main research objective has been to obtain the best catalytic performance in terms of stability, selectivity, CO_2 conversion, and CH_4 production, especially aimed at mild reaction conditions (i.e. low reaction temperature). Ru/TiO_2 catalyst is widely recognized as one of the most attractive formulation [15,24–29], allowing to obtain ~100% selectivity to methane when operating under mild reaction conditions (e.g. at atmospheric pressure and ~200 °C or lower). Yet, the structure-performance relationship appears to be a key

* Corresponding authors.
E-mail addresses: damien.debecker@uclouvain.be (D.P. Debecker), capucine.sassoye@upmc.fr (C. Sassoye).

http://dx.doi.org/10.1016/j.apcatb.2017.08.058
Received 22 May 2017; Received in revised form 7 August 2017; Accepted 17 August 2017
Available online 24 August 2017
0926-3373/

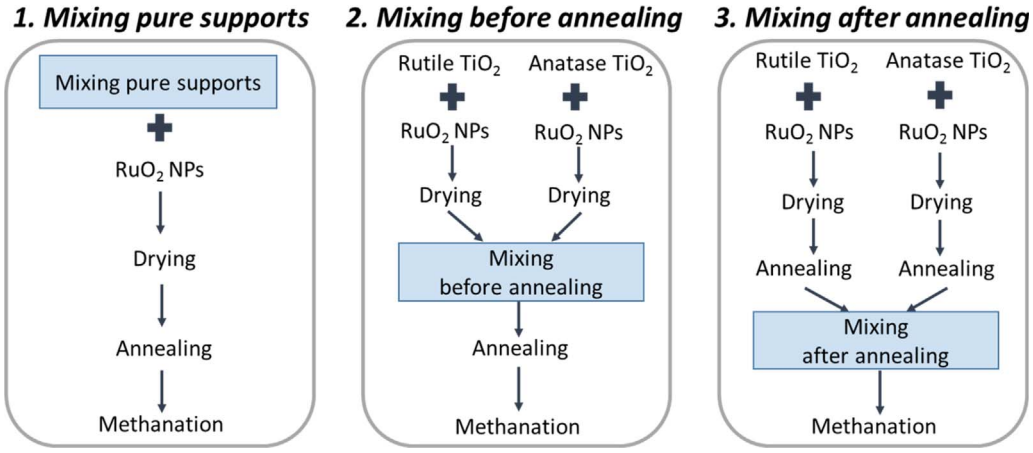

Fig. 1. Schematics of mixing anatase and rutile TiO_2 phases at different stages of catalyst preparation. The three routes are denoted "mixing 1", "mixing 2" and "mixing 3" in the following. Methanation step include in-situ reduction of RuO_2 into Ru.

for the development of high performance catalysts.

The crystal structure of TiO_2 support was shown to play an important role that dictates the morphology of Ru species, thereby affecting the catalytic performance in CO_2 methanation. In a recent contribution, we showed that Ru/TiO_2 catalyst supported on the commercial TiO_2-P25 from Degussa, which is composed of 20% rutile and 80% anatase phases, presents the highest catalytic performance compared to Ru/TiO_2 catalysts supported on pure anatase TiO_2 or rutile TiO_2 [24]. Our observations were in accordance with the previously reported studies in which highly dispersed and stable RuO_2 species were formed on rutile TiO_2 owing to the lattice matching with rutile TiO_2 support in HCl oxidation [30–32] and CO_2 methanation [28].

The high catalytic performance was found to be correlated to the high Ru dispersion, which itself was dictated by three phenomena [24]. First, thin layers of RuO_2 were formed on the rutile TiO_2 particles during annealing, owing to the lattice matching between rutile TiO_2 and rutile RuO_2 phases. These species generate highly dispersed Ru nanoparticles upon reduction [33]. This behavior is the opposite to the case of the anatase TiO_2 support onto which RuO_2 sinters heavily, leading to extremely low Ru dispersion in the final catalyst. Second, on the mixed support, we evidenced the migration of RuO_2 nanoparticles from anatase particles to rutile particles, where they maintained a good dispersion. Third, the homemade supports suffered from heavy sintering upon annealing which resulted in a significant loss of specific surface area and − more importantly − in the trapping of RuO_2 layers by sandwiching between rutile TiO_2 rods. Thus the mixed support allowed reaching higher performance because (i) it contained rutile TiO_2 particles which favor the dispersion of the Ru phase and (ii) it contains anatase TiO_2 particles from which Ru migrates, but which impede the sintering of rutile TiO_2 particles.

In this contribution, we present experimental data to elucidate the origin of such beneficial effect of mixing anatase and rutile. Ru/TiO_2 catalysts are prepared by deposition of pre-synthesized RuO_2 nanoparticles on mixtures of rutile and anatase TiO_2 with various mixing ratios while keeping other parameters constant (Ru loading and annealing condition). Rutile and anatase phases are mixed at three different stages of catalyst preparation, i.e. before RuO_2 deposition, before annealing, or after annealing. For those catalysts based on mixed supports at various ratio of rutile to anatase, we define "synergy" as the result of greater methane production rate as compared to the weighted average methane production rate of the pure rutile TiO_2 and pure anatase TiO_2 supported catalysts. We verify whether higher activity can be explained by the formation of more active Ru species or whether it is simply governed by dispersion. Both homemade and commercial rutile and anatase TiO_2 are exploited in an attempt to separate the crystalline structural effect from the effect of thermal stability (vs. sintering).

2. Experimental

2.1. Catalyst preparation

Homemade rutile and anatase TiO_2 supports were prepared as previously described [24]. The commercial TiO_2 nanopowder was obtained from Sigma-Aldrich; anatase nanopowder (99.7% trace metal basis, particle size < 25 nm) and rutile nanopowder (99.5% trace metal basis, particle size < 100 nm). A highly stable colloidal suspension of monodispersed RuO_2 nanoparticles [34,35] was obtained by a dropwise addition of 15%v/v H_2O_2 diluted in H_2O into 0.011 M $RuCl_3{\cdot}xH_2O$ (x = 3–5) dissolved in H_2O so that the final concentration of Ru ≈ 0.007 M. The solution was heated at 95 °C for 2 h. Once cooled to room temperature, an appropriate amount of TiO_2 powder was added to the colloidal suspension of RuO_2 nanoparticles to yield 2.2 wt.% of Ru in the final catalyst. The mixture was put in an oven at 50 °C overnight and the excess water was removed by rotary evaporation. The resulting powder was then calcined at 450 °C for 16 h in static air (this step is called "annealing" in the following).

To prepare catalysts based on the mixing of two pure supports, the mixing was done at different stages of the preparation. The schematics of catalyst preparation involving the mixing of anatase and rutile TiO_2 phases are shown in Fig. 1.

First, pure rutile and anatase supports were mechanically mixed in various mass ratios (rutile to anatase = 5:5, 3:7, 2:8, 1:9 for homemade TiO_2 supports and rutile to anatase = 5:5, 2:8 for commercial TiO_2 supports) followed by the deposition of RuO_2 NPs, drying and annealing. This procedure is referred to as "mixing 1". The catalysts are denoted as (R + A)55, (R + A)37, (R + A)28, and (R + A)19 for homemade TiO_2 supports and C(R + A)55 and C(R + A)28 for commercial TiO_2 supports respectively, where the numbers indicate the anatase-to-rutile mass ratio and "C" indicates the commercial origin of the supports.

Second, RuO_2 NPs were deposited and dried on rutile and anatase supports separately then mixed in various ratios right before annealing. This procedure is referred to as "mixing 2". The catalysts are noted (R + A)55-BA, (R + A)37-BA, (R + A)28-BA, and (R + A)19-BA for homemade TiO_2 supports and C(R + A)55-BA and C(R + A)28-BA for commercial TiO_2 supports, where "BA" stands for "before annealing".

Third, RuO_2 NPs were deposited and dried on rutile and anatase supports separately, annealed separately (i.e. the complete catalyst preparation procedure), and then mixed in various ratios. This procedure is referred to as "mixing 3". The catalysts are noted (R + A)55-AA, (R + A)37-AA, (R + A)28-AA, and (R + A)19-AA for homemade TiO_2 supports and C(R + A)55-AA and C(R + A)28-AA for commercial TiO_2 supports, where "AA" stands for "after annealing".

For comparison, pure anatase supported catalysts and pure rutile supported catalysts were prepared and denoted as A100 and R100 for

Table 1
Catalysts nomenclature, nominal support composition and preparation procedure.

Rutile content (%)	Anatase content (%)	Homemade TiO_2			Commercial TiO_2	
		Mixing 1	Mixing 2	Mixing 3	Mixing 1	Mixing 3
0%	**100%**	A100 (no mixing)			CA100 (no mixing)	
10%	**90%**	(R + A)19	(R + A)19-BA	(R + A)19-AA		
20%	**80%**	(R + A)28	(R + A)28-BA	(R + A)28-AA	C(R + A)28	C(R + A)28-AA
30%	**70%**	(R + A)37	(R + A)37-BA	(R + A)37-AA		
50%	**50%**	(R + A)55	(R + A)55-BA	(R + A)55-AA	C(R + A)55	C(R + A)55-AA
100%	**0%**	R100 (no mixing)			CR100 (no mixing)	

homemade anatase and rutile supported catalysts respectively and CA100 and CR100 for commercial anatase and rutile supported catalysts respectively. Table 1 summarizes the studied catalysts.

2.2. Catalyst characterization

ICP-AES elemental analysis of the catalysts resulted in Ru contents of 2.35–2.60 wt.%, indicating no Ru loss during the entire synthesis process (small variation comes from the variation in the water content in the RuCl3.xH2O (x = 3–5) precursor).

The specific surface area of the catalysts was obtained by nitrogen adsorption–desorption isotherm collected at −196 °C on a BELSORB-mini II (BEL Japan, Inc.). The samples were outgassed for overnight at 140 °C prior to the analysis. SBET was calculated applying the Brunauer, Emmet and Teller (BET) method for N_2 relative pressure in range of $0.05 < P/P_0 < 0.30$.

H_2 chemisorption at 100 °C was used to measure the exposed Ru atoms using ASAP 2010C apparatus from Micrometrics. Catalyst weight between 150 and 200 mg was loaded into a Pyrex tube, and subsequently degassed in He at 150 °C for 30 min. After evacuation, the sample was reduced in pure H_2 at 200 °C for 2 h (same as in situ reduction for methanation, see Section 2.3) followed by purging with He at 100 °C for 1 h and adsorption of H_2. Two isotherms were measured in the range of 0.08–95 kPa. The first accounts for reversible and irreversible chemisorption. The sample was evacuated to desorb reversibly adsorbed H_2. The second isotherm was then measured which accounts only for the reversibly adsorbed H_2. The subtraction of the linear part of the two isotherms gave the total amount of irreversibly adsorbed (chemisorbed) H_2. The amount of surface Ru atoms was calculated from the amount of chemisorbed H_2 assuming that the chemisorption stoichiometry is H:Ru = 1 [36]. It should be noted that the amount of surface Ru is possibly overestimated due to H_2 spillover on the titania support [37]. Reported values of dispersion − defined as surface Ru atoms divided by total Ru atoms in the catalyst − can be used to compare catalysts among each other but should not be taken as absolute numbers.

Transmission electron microscopy (TEM) images were obtained with a FEI Tecnai 120 Twin microscope, operating at 120 kV and equipped with a GatanOrius CCD numeric camera. The samples were prepared by ultrasonic dispersion of the powders in water and a droplet of the dispersion was then placed onto a carbon-coated copper grid.

High angle annular dark field scanning transmission electron microscopy (HAADF-STEM) images were obtained using a Jeol 2200FS microscope equipped with a spherical aberration corrector on the probe and an EDX system from Jeol.The convergence semi-angle of the probe was 30 mrad and the current was 150 pA. The inner and the outer semiangles for the dark-field detector (upper DF detector) were 100 and 170 mrad, respectively. The sample preparation was the same as described in TEM sample preparation.

X-ray diffraction (XRD) measurements were performed using Cu Kα radiation in a Bruker D8 Advance diffractometer equipped with a Lynx eye detector. The 2θ diffractograms were recorded between 24 and 50° with a step size of 0.04° and a steep time of 20 s/step. The ICDD-PDF2 database was used to identify the crystalline phases. Deconvolution of TiO_2 and RuO_2 XRD peaks was performed using WinPLOTR 2014 software [38]. The Scherrer equation [39] was used to calculate the crystallite size of TiO_2 particles. From TEM analysis, commercial particles and homemade pure anatase shows roughly isotropic shapes whereas homemade pure rutile TiO_2 particle crystalize as c-axis oriented needles. Thus, both commercial and homemade pure anatase TiO_2 particle sizes were evaluated taking into account all XRD peaks width. The (001) rutile diffraction peak being forbidden, no easy estimation of the homemade rutile TiO_2 needle length could be made. Rutile needle width was estimated from the (110) diffraction peaks.

2.3. Methanation reaction

200 mg of catalyst with particle size between 100 and 315 µm was loaded in a continuous flow fixed bed reactor and reduced in situ at 200 °C for 2 h under 30 ml/min of H_2 prior to the catalytic reaction. The reaction was carried out at 1 atm between 50 °C and 200 °C under a reaction mixture of 20 ml/min (CO_2 (10 vol.%), H_2 (40 vol.%) diluted in He). Considering the dilution and the low level of conversion, variations in flow rate due to the methanation reaction are neglected. Each temperature was maintained for 52 min (3 GC injections). The exit gases were quantified using a gas chromatograph (Varian CP3800), equipped with Hayesep Q, Molsieve 5A, and CP-Sil-5CB columns. The separated gases were detected with a flame ionization detector (CH_4) and a thermal conductivity detector (CO and CO_2). Analysis parameters were set as to allow an analysis each 19 min and to obtain measurements accurate within about 1% (relative) for the methane production rate (mole of methane produced per gram of catalyst per second). All transfer lines were maintained at 110 °C to avoid water condensation.

3. Results and discussion

3.1. Mixture of homemade anatase and rutile TiO_2

3.1.1. Activity of the catalysts obtained by mixing after annealing (Mixing 3)

In the chosen reaction conditions, the selectivity to methane for all catalysts was 100%. CO_2 conversion values are provided in the electronic supplementary information (ESI), in Table S1 and S2. Here, catalytic activities are discussed in terms of methane production rates, based on the mass of catalyst ($\mu mol_{CH4} \cdot g_{cat}^{-1}\ s^{-1}$). The activity of the catalysts obtained at different ratios of rutile: anatase mixing are shown as a function of anatase content in the catalysts (Fig. 2). The dotted lines represent the calculated weighted average activity of pure rutile TiO_2 supported catalyst and pure anatase TiO_2 supported catalyst.

For the catalysts mixed after being prepared and annealed separately on rutile and anatase TiO_2 supports (mixing 3), the catalytic activity of each mixing ratio corresponded closely to the weighted average of the activity of the pure rutile supported and anatase supported catalysts. This shows that there is no impact of the co-presence of rutile and anatase TiO_2 particles during reaction.

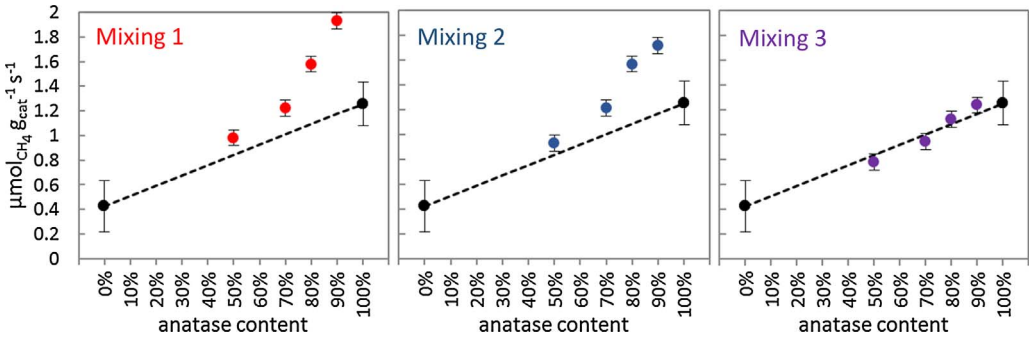

Fig. 2. Methanation rate for the three mixing series from homemade supports, as a function of the anatase content in the samples (red, blue, and purple data points). In each plot, the activity of R100 (0% anatase) and A100 (100% anatase) are shown with black dots. The dotted line indicates the calculated weighted average of R100 and A100 activities as if they were mixed at various ratios and under the hypothesis that they act independently at their respective rates. The error bars represent the statistic error (repeatability) of the catalytic testing procedure for one prepared catalyst. For R100 and A100, the error bar ranges also account for the preparation (reproducibility); two same catalysts were prepared separately with different batches of pure homemade TiO_2 and tested. (For interpretation of the references to color in this figure legend, the reader is referred to the web version of this article.)

3.1.2. Activity of the catalysts obtained by mixing before annealing (Mixing 2)

The RuO_2 nanoparticles were deposited separately on rutile and anatase TiO_2 supports and then the resulting materials were mixed before annealing. The catalytic activities were found to be significantly above the calculated weighted average activity line, as shown in Fig. 2 (center). In other words, the observed catalytic activity with the mixed catalysts was higher than the weighted average activity of the respective pure catalysts; there is a beneficial cooperation between the two mixed parts. Such beneficial effect is commonly called “synergy”. The synergistic effect was not obvious for (R + A)55-BA and (R + A)37-BA, but was evident for (R + A)28-BA and (R + A)19-BA.

3.1.3. Activity of the catalysts obtained by mixing before RuO_2 deposition (Mixing 1)

The catalysts were prepared by mixing rutile and anatase TiO_2 supports prior to RuO_2 nanoparticles deposition (Fig. 2, left). The synergy was observed in a similar manner as in the case of catalysts in mixing 2 series. Again, the synergy was especially significant with the catalysts obtained at mixing ratios 2:8 and 1:9. Interestingly, for each

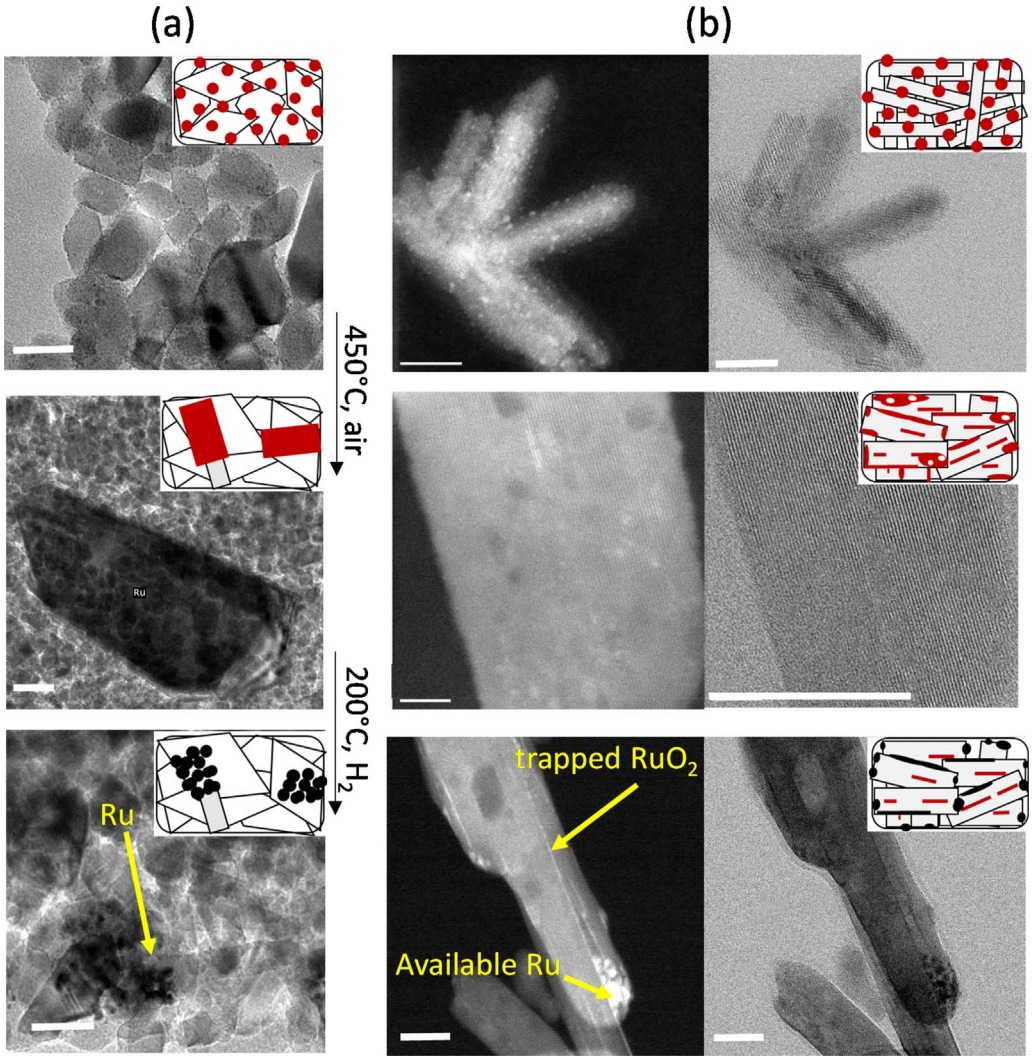

Fig. 3. Selected electron microscopy images representing the catalysts, from top to down, as synthesized, after annealing, and after methanation. (a) TEM images from A100 (catalyst obtained from the homemade pure anatase support), (b) STEM-HAADF and STEM-BF images from R100 (catalyst obtained from the homemade pure rutile TiO_2 support). The scale bars represent 20 nm.

Table 2
Textural properties of the homemade anatase and rutile TiO_2 supports and of the catalysts obtained from them (N_2 physisorption). Catalysts are characterized after annealing, prior to reduction and methanation.

	Surface area ($m^2\,g^{-1}$)	Pore volume ($cm^3\,g^{-1}$)
rutile TiO_2	79	0.19
anatase TiO_2	144	0.15
rutile TiO_2 calcined	32	0.14
anatase TiO_2 calcined	60	0.13
R100	27	0.14
A100	59	0.17
(R + A)55	48	0.16
(R + A)37	48	0.13
(R + A)28	60	0.14
(R + A)19	62	0.12
(R + A)55-BA	47	0.19
(R + A)37-BA	51	0.20
(R + A)28-BA	55	0.19
(R + A)19-BA	61	0.21
(R + A)55-AA	44	0.18
(R + A)37-AA	49	0.19
(R + A)28-AA	50	0.19
(R + A)19-AA	64	0.21

mixing ration, the synergy was systematically slightly more important for the catalysts of the mixing 1 series as compared to mixing 2.

3.1.4. Catalyst characterization

After impregnation of the colloidal suspension, RuO_2 nanoparticle are dispersed over the support particles (Fig. 3, top). After annealing, however, drastic modifications occur (Fig. 3, center) . On anatase TiO_2, heavy sintering of RuO_2 is observed. On rutile TiO_2, RuO_2 spreads in the form of thin layers on the surface of the particles or is "sandwiched" between sintered rutile TiO_2 rods. Upon reduction, large chunks of Ru are detected on anatase TiO_2, while small Ru particles are found on the surface of rutile TiO_2 rods, along with some RuO_2 which remains trapped in the sintered support (Fig. 3, bottom). These modifications are described in details in our previous work [24]. Also, when a mixture of anatase TiO_2 and rutile TiO_2 is used as a support for RuO_2 nanoparticles, RuO_2 migrates towards the rutile TiO_2 particles (supplementary information, Fig. S1). Here, the impact of these phenomena is inspected in details for different mixing ratios and mixing procedures.

The textural properties of the catalysts analyzed by N_2 physisorption are summarized in Table 2. The texture of the starting anatase and rutile supports (specific surface areas of ~ 140 $m^2\,g^{-1}$ and 80 $m^2\,g^{-1}$, respectively) is affected by the catalyst preparation, leading to corresponding Ru/TiO_2 catalysts with specific surface areas of ~60 $m^2\,g^{-1}$ and ~30 $m^2\,g^{-1}$, respectively. Expectedly, the mixing of both catalysts after annealing (mixing 3) produces catalysts with specific surface areas corresponding exactly to the weighted averages of the specific surface areas of the separate catalysts. It is noteworthy, however, that two other series of samples (mixing pure supports first and mixing before annealing) show similar specific surface areas, pointing to an absence of impact of the mixing stage to the TiO_2 sintering behavior. On the other hand, it is notable that, while the pore volumes are similar for the catalysts mixed before annealing (Mixing 2) and after annealing (Mixing 3), the catalysts prepared by mixing the pure supports prior to the RuO_2 NPs deposition (Mixing 1) systematically present smaller pore volumes. We put forward that a better degree of mixing of rutile and anatase particles is obtained in aqueous suspension as compared to mechanical grinding, which leads to a tighter contact among particles in the aggregates and smaller interparticle porosity.

A factor influencing catalytic activity is the Ru dispersion, namely the proportion of Ru atoms effectively accessible on the surface of the catalyst and thus potentially active in the reaction. Ru dispersion has been measured by H_2 chemisorption for the catalysts made from pure anatase and rutile TiO_2 supports as well as for the mixtures (Fig. 4).

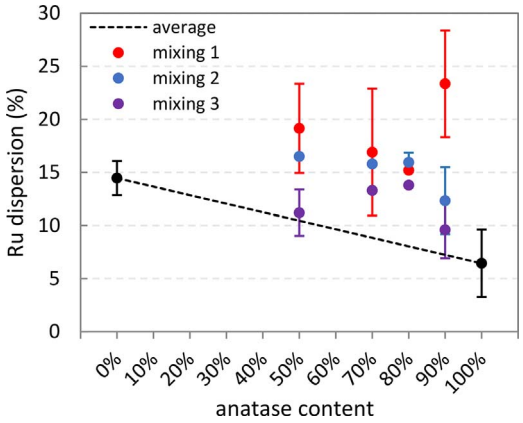

Fig. 4. Ru dispersion (%) obtained by number of surface Ru atoms probed by H_2 chemisorption divided by total number of Ru atoms catalyst determined by ICP-AES. A100 and R100 are shown as references with error ranges determined from several reproduced catalysts. (For interpretation of the references to color in this figure legend, the reader is referred to the web version of this article.)

The anatase supported Ru catalyst displayed a much lower dispersion than the catalyst prepared from pure rutile. This is explained by a heavy sintering of RuO_2 when supported on anatase (Fig. 3). On rutile, TEM reveals that RuO_2 was in part highly dispersed at the surface of rutile rods (stabilized through epitaxial interactions) and in part trapped ("sandwiched") between rutile rods that tend to sinter during annealing (Fig. 3). Both phenomena are expected to have opposite effect on the dispersion value. Yet the dispersion value for rutile supported catalyst (R100) reached ~14%, significantly higher than that of the anatase supported catalyst (A100).

Catalysts from the mixing 3 series tend to exhibit Ru dispersion in the vicinity of the value expected for a simple mechanical mixture of R100 and A100. Catalysts from mixing 2 and mixing 1 series tend to exhibit higher dispersion. It is reasonable to consider that the "sandwiching" effect observed for R100 would be reduced in the case of an intimate mixture between anatase and rutile. Also, the migration of RuO_2 from anatase TiO_2 towards rutile TiO_2–discussed in details in our previous study [24] – is expected to occur in these samples, which should favor a better dispersion.

XRD patterns of all catalysts are presented in the supplementary information, Fig. S2-4. For conciseness, only the patterns of the catalysts prepared with the mixing ratio 2:8 rutile:anatase using the three mixing procedures are compared in Fig. 5. As expected, the patterns mainly show the presence of anatase and rutile TiO_2 phases (with a small amount of brookite phase in some cases) and in some catalysts, the presence of RuO_2 can be detected as a shoulder to the rutile TiO_2 peaks. The intensities of the rutile and anatase TiO_2 peaks consistently follow the nominal composition (Fig. S2-4). XRD peaks associated with RuO_2 are visibly more pronounced on the catalyst prepared by mixing after annealing (Fig. 5). While RuO_2 peaks are too small in intensity to be refined using a pattern matching method, the position and width of the main TiO_2 and RuO_2 peaks for each catalyst could be obtained after deconvolution. Results are reported in Table S3. Overall, TiO_2 peak positions and widths (2θ and FWHM) do not evolve when the mixing order or the anatase/rutile ratio is changed; mixing order or anatase/rutile ratio do not influence the TiO_2 sintering in comparison to what already occurs on pure homemade TiO_2 supported RuO_2 catalysts, nor do they influence the crystal structure (cell parameters) of the TiO_2 supports.

On the other hand, the RuO_2 peak positions appear to evolve. For a better visualization of the shifts in RuO_2 peak positions, the 110 2θ positions were subtracted from the 101 2θ positions and compared with the expected value ($2\theta_{101}$–$2\theta_{110}$ = 7.024° for RuO_2 as per ICDD 01-070-2662), as shown in Fig. 6(a). The mixing 3 series of catalysts show values close to this expected value. Upon annealing prior to mixing, the

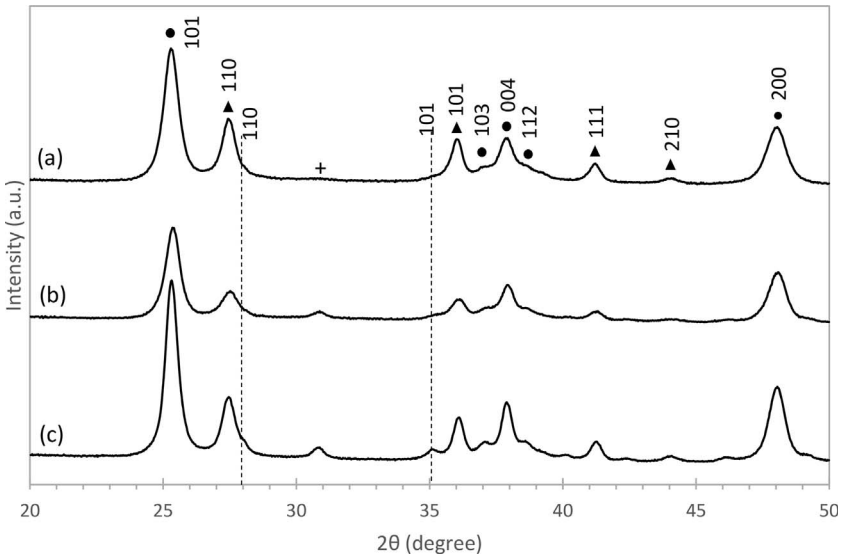

Fig. 5. XRD patterns of (a) (R + A)28, (b) (R + A)28-BA, (c) (R + A) 28-AA from homemade supports; rutile TiO_2 (▲), anatase TiO_2 (●), brookite TiO_2 (+), and rutile RuO_2 (drawn as dotted lines) peak positions.

RuO_2 nanoparticles grow into larger RuO_2 crystals independently from the support on anatase TiO_2, while they transform into epitaxial layer over rutile TiO_2 in strong interaction with the support [24]. When these two catalysts were mixed (mixing 3) two RuO_2 peaks can expected: one which is thin and non-shifted (on anatase), and one which is broad and shifted toward TiO_2 rutile peak positions (on rutile). The former dominates the diffractogram and relatively broad un-shifted peaks are observed.

On the contrary, the mixing 2 and 1 series clearly show significantly higher values for the RuO_2 $2\theta_{101}$-$2\theta_{110}$ difference, attesting of a change in the RuO_2 structure towards rutile TiO_2 structure. In these samples, both RuO_2 peaks are shifted towards the associated rutile TiO_2 peaks. This is consistent with the fact that RuO_2 nanoparticles are able to migrate from anatase TiO_2 to rutile TiO_2 during annealing and to form epitaxial layers. The effect is larger for mixing 1 than mixing 2. We hypothesize that this results from a better degree of mixing with higher proximity between rutile and anatase particles at the wet step of the preparation, which may facilitate RuO_2 nanoparticles migration.

In comparison, Fig. 6(b) shows the values of the difference in $2\theta_{101}$ and $2\theta_{110}$ positions of rutile TiO_2, which always remain close to the expected value of 8.639° (as per ICDD 00-021-1276), attesting that the support is not affected by these phenomena.

The size of RuO_2 is difficult to evaluate by XRD due to the low peak intensity, their overlapping with rutile TiO_2 peaks, as well as the fact that RuO_2 is well known to present numerous defects which enlarge the XRD peaks by itself [40].

3.1.5. Interpretation of the synergistic effect

Based on the catalytic activities of the mixing 3 series that systematically fall on the weighted average activity of the R100 and A100 at all mixing ratios, the synergy in the catalytic activities clearly does not simply come from the co-presence of the two different TiO_2 phases during the reaction. Instead, the synergy observed for mixing 1 and 2 is the result of the co-existence of the two different TiO_2 phases during annealing. The co-existence of rutile and anatase supports in the annealing step dictates the localization and morphology of the RuO_2 and then Ru particles that are stabilized on the support upon reduction.

It is important to note that the activation energies for all catalysts were similar (Table 3 and Fig. S5-7). This indicates that the rate determining pathway of the catalytic reaction and the nature of the active sites are the same for all catalysts. It must be recalled that the rate limiting step in CO_2 methanation is the dissociation of adsorbed CO (formed after a first rapid dissociation of CO_2) [3,10,41]. Thus the factor dictating the activity of the catalysts is the number of surface sites able to catalyze the dissociation of adsorbed CO. This is obviously influenced by the dispersion, i.e. the available metallic surface. However, it may also depend on Ru particle size (the number of sites that turn out to be active in the reaction depend on the curvature of the particle [42]) or on the formation of specific sites at the interface between the metallic particles and the support (e.g. oxygen vacancy located at the metal-support interface, which are often proposed to take an active part in the rate limiting step [43,44]).

In an attempt to explain the performance of the catalysts by the dispersion of the active phase, the methanation activity has been normalized by the amount of surface accessible Ru atoms (probed by H_2-

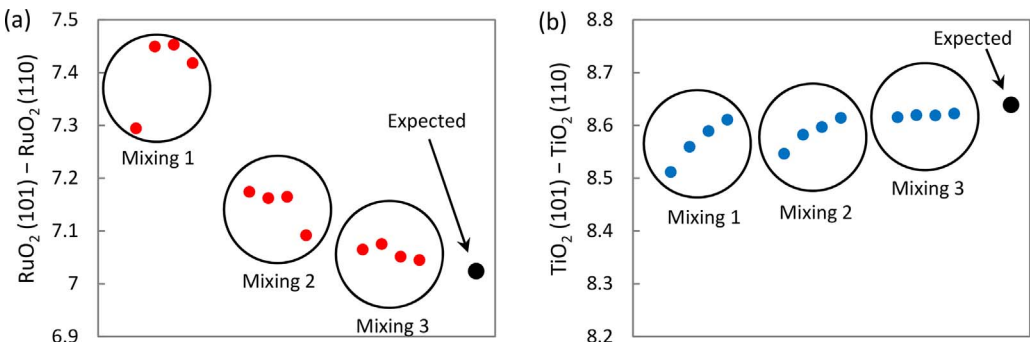

Fig. 6. The difference in the XRD 2θ peak positions, 101 and 110, for (a) RuO_2 and (b) rutile TiO_2. Expected values are taken from ICDD 01-070-2662 for RuO_2 and ICDD 00-021-1276 for rutile TiO_2. The grouped four data points represent rutile to anatase mixing ratios, 1:9, 2:8, 3:7, 5:5, from left to right.

Table 3
Summary of activation energies (Ea) of the catalysts prepared from home-made supports (see also Arrhenius plots in Fig. S5-7).

rutile:anatase ratio	Mixing 1 (R + A)	Mixing 2 (R + A)-BA	Mixing 3 (R + A)-AA
5:5	16.2	15.5	15.0
3:7	16.5	15.5	15.1
2:8	15.2	14.9	15.2
1:9	15.3	15.1	15.1

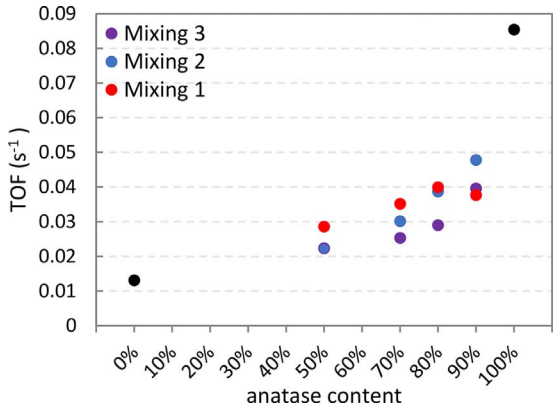

Fig. 7. Turn over frequencies (TOF) for all catalysts prepared from homemade supports. The TOF is calculated as the methane production rates normalized by the surface Ru (itself probed by H2 chemisorption). (For interpretation of the references to color in this figure legend, the reader is referred to the web version of this article.)

chemisorption). This provides the apparent TOF, here defined as the number of methane molecule produced per surface Ru atom and per second (Fig. 7). A100 has a specific activity 3-times higher than R100 and its dispersion is 3 times lower. Thus, the TOF of A100 is about 1 order of magnitude higher than that of R100. This shows that activity is not simply governed by dispersion. Indeed, in such case, the TOF would be the same for both catalysts. Instead, such marked difference in TOF points to a marked difference in the speciation of surface Ru atoms in both catalysts. For a given surface of Ru atoms, those that are found on the large Ru aggregates formed on anatase supported catalysts are ~10 times more abundant than those found on the smaller Ru particles formed on rutile supported catalysts.

Consistent with the migration of ruthenium from anatase particles to rutile particles, TOF values were systematically found in the interval between the extreme values of R100 and A100. TOF tends to increase as the anatase content increases (Fig. 7). No clear delineation can be drawn between the catalysts from the three mixing series. The TOF values land in the same area, not far from the theoretical line, but systematically lower (closer to R100 than A100). Within the hypothesis that all the RuO_2 migrates towards rutile and subsequently forms

Table 4
Textural properties of the catalysts prepared from the commercial anatase and rutile TiO_2 supports (N_2-physisorption).

	Surface area ($m^2\ g^{-1}$)	Pore volume ($cm^3\ g^{-1}$)
rutile TiO_2	48	0.25
anatase TiO_2	21	0.08
rutile TiO_2-calcined	48	0.25
anatase TiO_2-calcined	23	0.08
CR100	42	0.21
CA100	24	0.09
C(R + A)55	34	0.29
C(R + A)28	40	0.26
C(R + A)55-AA	35	0.29
C(R + A)28-AA	41	0.27

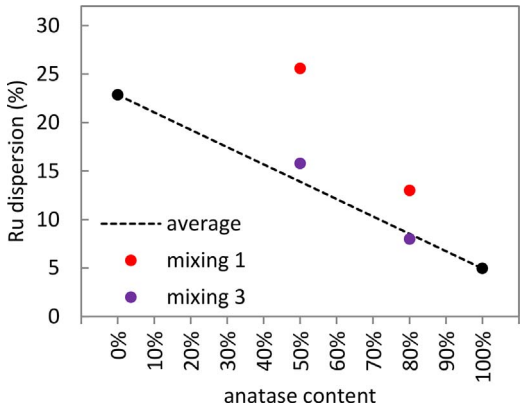

Fig. 9. Ru dispersion (%) of catalysts prepared with non-sintering commercial TiO_2. CA100 and CR100 are shown as References. (For interpretation of the references to color in this figure legend, the reader is referred to the web version of this article.)

identical rutile-supported Ru nanoparticles, in all catalysts prepared by support mixing before annealing, one should expect a constant TOF, close to that obtained for R100. However, as mentioned above, it is clear that the intrinsic activity of surface Ru is also affected by other factors like the particle size or the nature of the interaction with the support. As Ru concentrates on rutile particles (especially in anatase-rich mixtures), the Ru particles size is expected to be affected, potentially leading to a different TOF. Also, if a fraction of the Ru did not migrate and still formed large Ru chunks as those formed in A100, the measured dispersion (and the corresponding TOF) should be an average of both types of active species. Finally, let us remember that rutile rods stacking with the sandwiching of RuO_2 was clearly observed. It is possible that mixed support tend to minimize this phenomenon. Taking into consideration the absence of clear trend in this set of data, no hasty conclusion should be drawn on the TOF.

At this point, we conclude that the beneficial effect of mixing

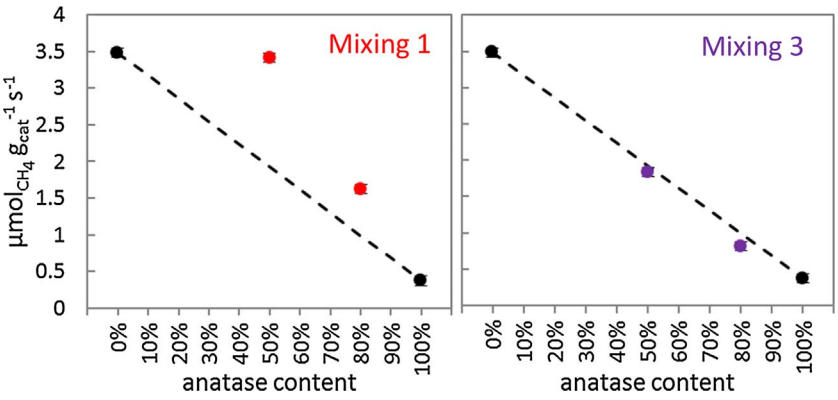

Fig. 8. Methanation production rate as a function of the anatase content. CR100 and CA100 are shown in black dots, the dotted line indicates the weighted average of CR100 and CA100 activities as if they were mixed at various ratios. The (very small) error bars show the repeatability of the catalytic testing apparatus. (For interpretation of the references to color in this figure legend, the reader is referred to the web version of this article.)

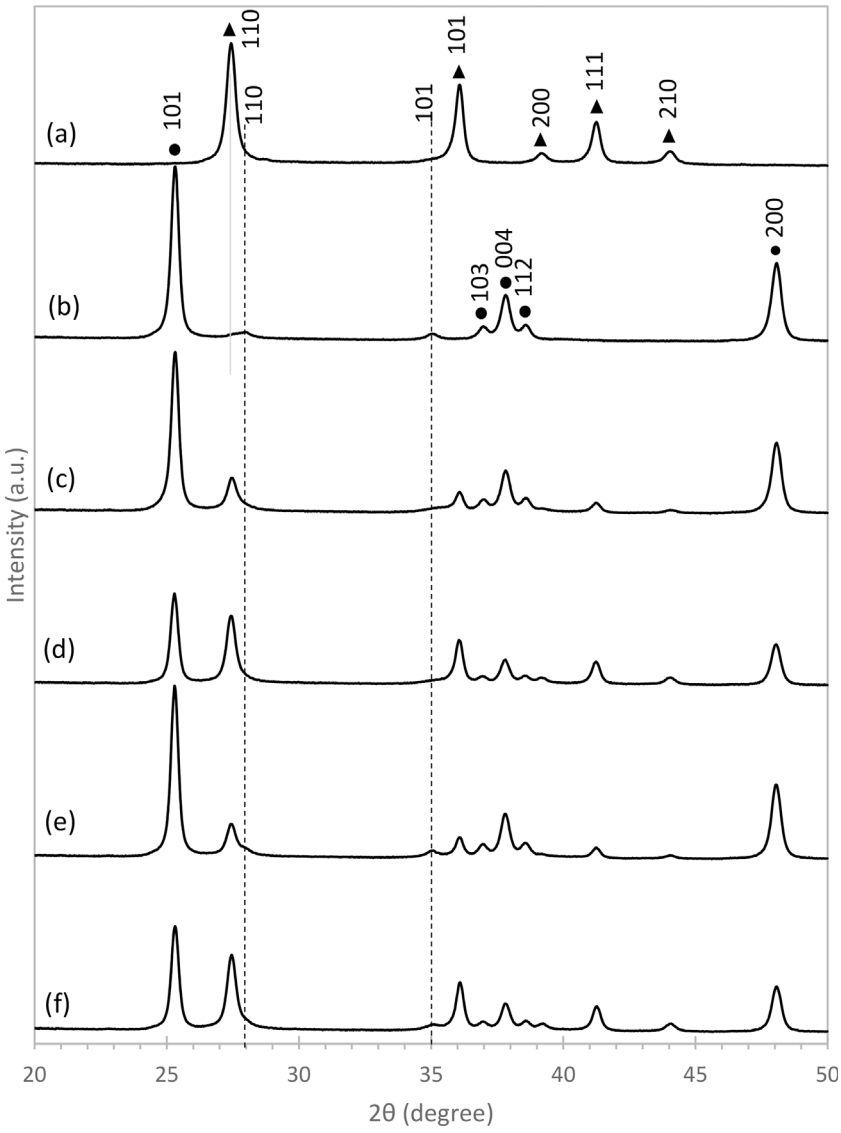

Fig. 10. XRD patterns of (a) CR100, (b) CA100, (c) C(R + A)28, (d) C(R + A)55, (e) C(R + A)28-AA, and (f) C(R + A)55-AA obtained from commercial supports; rutile TiO_2 (▲), anatase TiO_2 (●), and rutile RuO_2 (drawn as dotted lines) peak positions.

anatase and rutile in the preparation of Ru/TiO_2 catalysts arises from the co-presence of the two crystalline phases during annealing. RuO_2 does migrate from anatase TiO_2 to rutile TiO_2 support particles during the annealing step. Simultaneously, the loss of Ru through the TiO_2-RuO_2-TiO_2 particle stacking on the (110) facets may be partly prevented by the mixing of rutile and anatase TiO_2 particles, especially when diluting rutile in large proportions of anatase. Thus, the superior activity of catalysts based on mixed supports may be explained by a higher amount of surface Ru as compared to R100. However, it is not excluded that more active (larger) Ru metallic particles are formed due to the accumulation of higher Ru content on rutile particles. The heavy sintering observed with the homemade supports complicates drawing conclusions.

3.2. Mixture of commercial anatase and rutile TiO_2

In order to consolidate our interpretation of the synergy effect between anatase and rutile, a second set of experiments was carried out with commercial TiO_2 supports that do not sinter. Unlike the homemade supports, the commercial supports are stable after a 450 °C thermal treatment, even in the presence of Ru (see Section 3.2.2.). We study catalysts prepared by the mixing at the beginning or at the end of the preparation (mixing 1 and mixing 3) recalling that mixing 2 was shown to be equivalent to mixing 1. We compare them to the catalysts made from the pure commercial supports CR100 and CA100.

It should be noted that the catalytic activities of the catalysts prepared from the commercial anatase and rutile supports (CA100 and CR100) show completely opposite trend from what we have observed for A100 and R100: the catalytic activity of the catalyst based on commercial rutile TiO_2 is much higher than that based on commercial anatase TiO_2 (Fig. 8). CR100 was also more active than the catalyst based on the commercial P25 support [24]. This is consistent with earlier reports by Lin et al., who identified a non-sintering rutile TiO_2 support as the most promising for the design of methanation catalysts [28]. Indeed, in the case of stable rutile support, the interaction between RuO_2 and rutile TiO_2 is still favorable, but no Ru is lost by "sandwiching" between rutile TiO_2 rods.

3.2.1. Activity of the catalysts obtained by mixing (mixing 1 vs. mixing 3)

As expected, when the rutile TiO_2-supported and anatase TiO_2-supported Ru catalysts were mixed together after annealing, the catalytic activities of the mixed catalysts corresponded exactly to the weighted average activity of the two separately prepared CR100 and CA100 (Fig. 8, right). This is the same trend seen in the case of homemade TiO_2 supports and it indicates that the co-presence of rutile and anatase phases during reaction does not have any effect on the

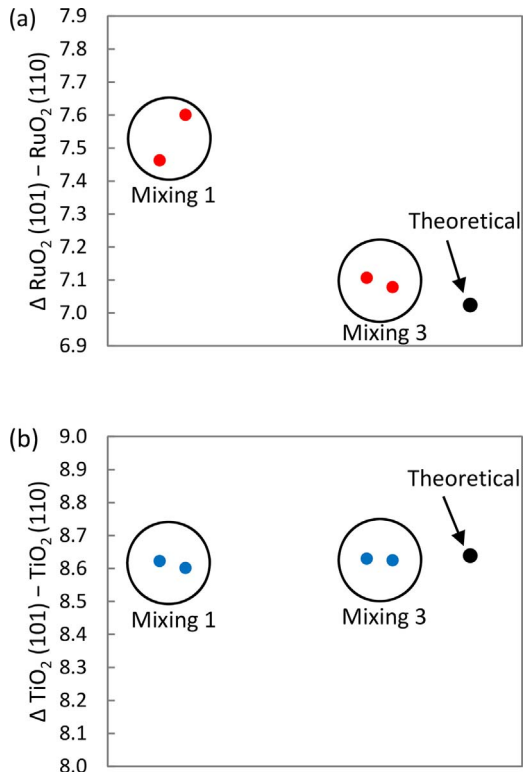

Fig. 11. The difference in the XRD 2θ peak positions, 101 and 110, for (a) RuO_2 and (b) rutile TiO_2. Expected values are taken from ICDD 01-070-2662 for RuO_2 and ICDD 00-021-1276 for rutile TiO_2.

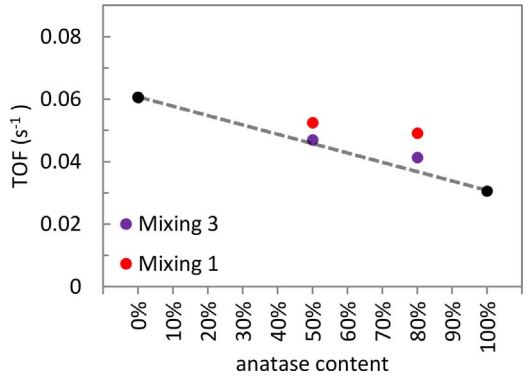

Fig. 12. Turn over frequencies (TOF) or methane production rates normalized per surface Ru probed by H_2 chemisorption for all catalysts concerned in this section. (For interpretation of the references to color in this figure legend, the reader is referred to the web version of this article.)

Table 5
Summary of activation energies (Ea) of the catalysts prepared from commercial supports (see also Arrhenius plots in Fig. S8-9).

rutile:anatase ratio	Mixing 1 C(R + A)	Mixing 3 (CR + A)-AA
5:5	14.6	15.0
2:8	14.6	14.4

activity.

When the mixing was done early in the preparation, the effect of synergy was observed (Fig. 8, left), confirming the beneficial effect of the co-presence of rutile and anatase during the annealing step. The catalytic activity reached the same activity as CR100 when the mixing ratio was 50% rutile to 50% anatase (C(R + A)55), significantly higher than the value expected for a simple mechanical mixture.

3.2.2. Catalysts characterization

N_2-physisorption analysis confirmed that both commercial anatase and rutile TiO_2 particles are not subjected to sintering upon annealing, with or without the presence of RuO_2 NPs, as shown in Table 4. The specific surface areas of the mixture of rutile and anatase phases at different catalyst preparation stages were unaffected and remained similar to the weighted averages of 50:50 mixture (33 $m^2\,g^{-1}$) and 20:80 mixture (38 $m^2\,g^{-1}$). Pore volumes were also unaffected by mixing at different stages.

The Ru dispersion on the commercial rutile TiO_2 is much higher than on the commercial anatase TiO_2 (Fig. 9). This again points to the heavy sintering of RuO_2 on anatase while a much better dispersion is obtained on rutile, thanks to the epitaxial stabilization effect. Dispersion for the mixing 3 series expectedly falls close to the values expected (weighted average) for simple mechanical mixtures of CR100 and CA100. On the other hand, the mixing 1 series appears to exhibit relatively high dispersion, clearly above that expected for mechanical mixture. Again, this points to a better dispersion when RuO_2 has the opportunity to migrate towards rutile during the annealing phase, while it sinters heavily when the only available support surface is anatase. Note that the dispersion obtained for C(R + A)55 is similar to that of R100. In the case of a quantitative migration of RuO_2 towards rutile, this suggests that similar Ru particles, with similar size are stabilized.

The XRD patterns of CR100 and CA100 are shown in Fig. 10. Similar behavior as the homemade TiO_2 supports was observed. On rutile TiO_2 support, only a slight broadening at each shoulder of rutile TiO_2 (110) and (101) peaks can be seen. On the other hand, on anatase TiO_2 support, RuO_2 (110) and (101) peaks are clearly visible, confirming the crystal growth of large RuO_2 crystals as on the homemade anatase TiO_2.

The XRD patterns of all commercial TiO_2 supported catalysts mixed at different stages of mixing in various ratios are shown together in Fig. 10 and the corresponding deconvolution results of the main TiO_2 peaks and RuO_2 peaks are summarized in Table S4. The difference in the positions of the 110 and 101 peaks of RuO_2 and rutile TiO_2 is plotted in Fig. 11. The same tendency was observed as in the previous section: (i) the 110 and 101 rutile TiO_2 peak positions remain constant regardless of the mixing order, and (ii) the shift in 110 and 101 RuO_2 peak positions towards 110 and 101 rutile TiO_2 peak positions is apparent for mixing 1 but not for mixing 3.

3.2.3. Interpretation of the synergistic effect

Synergy is confirmed: when a mixture of anatase and rutile is present during annealing, the specific activity is much higher than the expected value for simple mechanical mixtures. This is clearer in the present case because no support sintering is occurring. So the beneficial effect of support blending is not merely related to the absence of Ru "sandwiching". In theory, it can be the effect of two phenomena that are related to the migration of RuO_2 from anatase TiO_2 to rutile TiO_2.

Firstly, RuO_2 can migrate towards rutile TiO_2 when present, be stabilized via epitaxial interactions and − unlike when on anatase − remain highly dispersed after annealing and reduction. We propose to call this a "migration effect" which simply relates to the localization of ruthenium: on anatase it forms large chunks of RuO_2 with low specific activity but on rutile it forms dispersed Ru nanoparticles with high specific activity. Secondly, the higher concentration of Ru found on the rutile particles after migration can lead to larger Ru particles. We propose to call this a "concentration effect", accounting for the fact that − in a certain size range (a few nanometers) − larger Ru particles can have higher intrinsic activity. So even if dispersion is slightly lower than in R100, the activity can in principle be as high or even higher, simply because the morphology of the stabilized particles is different.

In attempt to discriminate between both effects, the apparent TOF was calculated by normalizing the activity by the amount of surface Ru (Fig. 12). It is noteworthy that the TOF for the pure commercial support

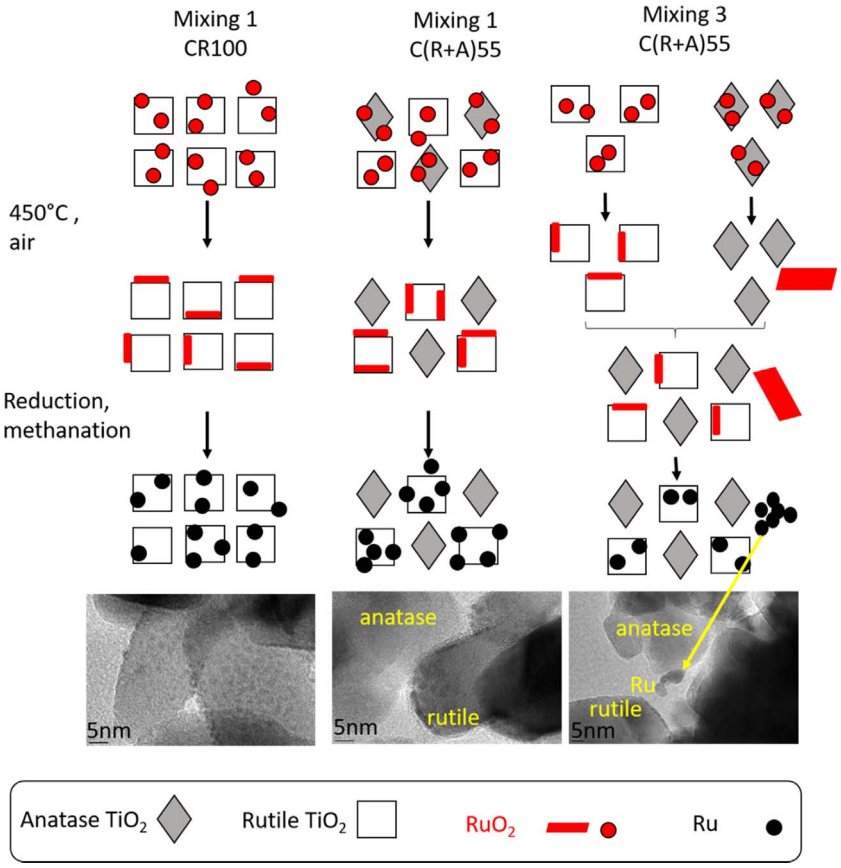

Fig. 13. Graphical representation and TEM images of Ru/TiO_2 methanation catalysts prepared from commercial supports; comparison between the catalysts based on pure rutile and those based on a mixture of anatase and rutile using either the "mixing1" or the "mixing 3" procedures. Mixing 1 permits the migration of RuO_2 towards the rutile TiO_2 particles and leads a situation similar to that obtained with pure rutile TiO_2 (anatase particles are spectators).

is different from that reported for the pure homemade supports. This again points to an influence of the interaction of the Ru nanoparticles with the TiO_2 supports (which can be linked to the formation of active sites). It would not be surprising that the nature of such interactions is different in the catalysts which undergo severe support modifications (sintering) vs. in the catalysts based on very stable supports. Nevertheless, the activation energies of the catalysts supported on commercial TiO_2 (Table 5 and Fig. S8-9) were similar to the catalysts supported on homemade TiO_2 (Table 3) at all different ratios of mixing at different steps. This indicates that the rate determining pathway of the catalytic reaction is the same for all catalysts.

For the catalysts prepared by mixing the final catalysts (Mixing 3), the TOF was close to the expected value for a simple mechanical mixture (as expected). For the catalyst prepared by mixing the pure supports before RuO_2 deposition and annealing (Mixing 1), the TOF values fell between the values of catalysts from Mixing 3 and that of CR100. This suggests that the main effect of synergy is simply related to the better Ru dispersion after migration towards rutile TiO_2 (migration effect) and not to the formation of another type of Ru particles that would exhibit a higher surface density of active sites (concentration effect). Fig. 13 sums up the interpretation that the non-sintering rutile TiO_2 support contributes to stabilize high Ru dispersion which leads to high methane production rate.

4. Conclusion

Ru/TiO_2 catalysts were prepared by a colloidal method, using RuO_2 nanoparticles in suspension as the precursor for the active phase and using mixtures of rutile and anatase TiO_2 as supports. The mixing of the two supports was done in various ratios and at different stages of catalyst preparation, i.e. before or after RuO_2 deposition, and after annealing. The catalysts were studied in the methanation of CO_2 after undergoing a thermal reduction under H_2. Activity depended markedly on the crystalline structure of the support. Catalysts prepared from mixed supports behaved differently, depending on the step at which rutile and anatase TiO_2 are combined. If the mixing is done after annealing, the activity simply corresponds to the weighted average activity of the two catalysts prepared from pure supports. The co-existence of rutile and anatase TiO_2 crystal phases during the reaction itself do not affect the catalytic performance. If, on the opposite, the mixing is done prior to annealing, a synergy is obtained: the catalyst based on a mixed support is significantly more active than the weighted average activity of the two catalysts prepared from pure supports. Characterization indicates that RuO_2 nanoparticles migrate towards the rutile TiO_2 phase to be stabilized by epitaxy. The stabilized RuO_2 phase located on rutile TiO_2 is then transformed into reduced Ru species exhibiting a high dispersion and high specific activity. In the catalysts prepared from homemade rutile and anatase TiO_2 supports, the blending is also beneficial to impede the negative effect of support sintering and especially the loss of Ru in TiO_2-RuO_2-TiO_2 "sandwich" structures. When thermally stable supports are used, the activity of the catalysts obtained by mixing the supports before annealing tend to reach the activity of the catalysts based on pure rutile. All in all, non-sintering rutile TiO_2 appears to be the best support to prepare highly active Ru/TiO_2 CO_2 methanation catalysts.

Acknowledgements

A.K. thanks the European doctoral school IDS FunMat fort the PhD fellowship. The authors acknowledge *Wallonie-Bruxelles International*, the *Ministère Français des Affaires étrangères et européennes* and the *Ministère de l'Enseignement Supérieur et de la Recherche* for their financial support in the framework of the Hubert Curien partnership (Tournesol), as well as *Gilles Patriarche* from Centre de Nanosciences et de Nanotechnologies, Université Paris-Saclay, C2N – Site de Marcoussi for STEM-HAADF images (Figs. 3b and Fig. S1). Authors also acknowledge the *Fondation Collège de France*.

Appendix A. Supplementary data

Supplementary data associated with this article can be found, in the online version, at http://dx.doi.org/10.1016/j.apcatb.2017.08.058.

References

[1] T.P. Senftle, E.A. Carter, Acc. Chem. Res. 50 (2017) 472–475.
[2] S.N. Riduan, Y. Zhang, Dalton Trans. 39 (2010) 3347–3357.
[3] W. Wei, G. Jinlong, Front. Chem. Sci. Eng. 5 (2011) 2–10.
[4] W. Wang, S. Wang, X. Ma, J. Gong, Chem. Soc. Rev. 40 (2011) 3703–3727.
[5] H. Yang, Z. Xu, M. Fan, R. Gupta, R.B. Slimane, A.E. Bland, I. Wright, J. Env. Sci. 20 (2008) 14–27.
[6] S. Kattel, P.J. Ramírez, J.G. Chen, J.A. Rodriguez, P. Liu, Science 355 (2017) 1296–1299.
[7] J. Wei, Q. Ge, R. Yao, Z. Wen, C. Fang, L. Guo, H. Xu, J. Sun, Nat. Commun. 8 (2017) 15174.
[8] F. Studt, I. Sharafutdinov, F. Abild-Pedersen, C.F. Elkjær, J.S. Hummelshøj, S. Dahl, I. Chorkendorff, J.K. Nørskov, Nat. Chem. 6 (2014) 320–324.
[9] C.V. Picasso, D.A. Safin, I. Dovgaliuk, F. Devred, D. Debecker, H.-W. Li, J. Proost, Y. Filinchuk, Int. J. Hydrogen Energy 41 (2016) 14377–14386.
[10] M.A.A. Aziz, A.A. Jalil, S. Triwahyono, A. Ahmad, Green Chem. 17 (2015) 2647–2663.
[11] M. Mikkelsen, M. Jorgensen, F.C. Krebs, Energy Env. Sci. 3 (2010) 43–81.
[12] O. Ola, M. Mercedes Maroto-Valer, S. Mackintosh, Energy Procedia 37 (2013) 6704–6709.
[13] G. Centi, S. Perathoner, Catal. Today 148 (2009) 191–205.
[14] T. Schaaf, J. Grünig, M.R. Schuster, T. Rothenfluh, A. Orth, Energy Sustain. Soc. 4 (2014) 2.
[15] P. Frontera, A. Macario, M. Ferraro, P. Antonucci, Catalysts 7 (2017) 59.
[16] J. Martins, N. Batail, S. Silva, S. Rafik-Clement, A. Karelovic, D.P. Debecker, A. Chaumonnot, D. Uzio, Catal. Commun. 58 (2015) 11–15.
[17] Y. Zhu, S. Zhang, Y. Ye, X. Zhang, L. Wang, W. Zhu, F. Cheng, F. Tao, ACS Catal. 2 (2012) 2403–2408.
[18] L. Roldán, Y. Marco, E. García-Bordejé, ChemSusChem (2016) (n/a-n/a).
[19] J. Zheng, C. Wang, W. Chu, Y. Zhou, K. Köhler, ChemistrySelect 1 (2016) 3197–3203.
[20] A. Karelovic, P. Ruiz, ACS Catal. 3 (2013) 2799–2812.
[21] A. Karelovic, P. Ruiz, J. Catal. 301 (2013) 141–153.
[22] H.Y. Kim, H.M. Lee, J.-N. Park, J. Phys. Chem. C 114 (2010) 7128–7131.
[23] J.H. Kwak, L. Kovarik, J. Szanyi, ACS Catal. 3 (2013) 2449–2455.
[24] A. Kim, C. Sanchez, G. Patriarche, O. Ersen, S. Moldovan, A. Wisnet, C. Sassoye, D.P. Debecker, Catal. Sci. Technol. 6 (2016) 8117–8128.
[25] C. Sassoye, G. Muller, D.P. Debecker, A. Karelovic, S. Cassaignon, C. Pizarro, P. Ruiz, C. Sanchez, Green Chem. 13 (2011) 3230–3237.
[26] T. Abe, M. Tanizawa, K. Watanabe, A. Taguchi, Energy Env. Sci. 2 (2009) 315–321.
[27] K.P. Brooks, J. Hu, H. Zhu, R.J. Kee, Chem. Eng. Sci. 62 (2007) 1161–1170.
[28] Q. Lin, X.Y. Liu, Y. Jiang, Y. Wang, Y. Huang, T. Zhang, Catal. Sci. Technol. 4 (2014) 2058–2063.
[29] G. Gouget, D.P. Debecker, A. Kim, G. Olivieri, J.-J. Gallet, F. Bournel, C. Thomas, O. Ersen, S. Moldovan, C. Sanchez, S. Carenco, D. Portehault, Inorg. Chem. 56 (2017) 9225–9234.
[30] E.V. Kondratenko, A.P. Amrute, M.-M. Pohl, N. Steinfeldt, C. Mondelli, J. Perez-Ramirez, Catal. Sci. Technol. 3 (2013) 2555–2558.
[31] K. Seki, Catal. Surv. Asia 14 (2010) 168–175.
[32] G. Xiang, X. Shi, Y. Wu, J. Zhuang, X. Wang, Sci. Rep. 2 (2012) 801.
[33] S. Carenco, C. Sassoye, M. Faustini, P. Eloy, D.P. Debecker, H. Bluhm, M. Salmeron, J. Phys. Chem. C 120 (2016) 15354–15361.
[34] D.P. Debecker, B. Farin, E.M. Gaigneaux, C. Sanchez, C. Sassoye, Appl. Catal. A 481 (2014) 11–18.
[35] C. Fernández, C. Sassoye, D.P. Debecker, C. Sanchez, P. Ruiz, Appl. Catal. A 474 (2014) 194–202.
[36] J. Okal, M. Zawadzki, L. Kępiński, L. Krajczyk, W. Tylus, Appl. Catal. A 319 (2007) 202–209.
[37] T. Komaya, A.T. Bell, Z. Wengsieh, R. Gronsky, F. Engelke, T.S. King, M. Pruski, J. Catal. 149 (1994) 142–148.
[38] T. Roisnel, J. Rodirguez-Carvajal, WinPLOTR, a Graphic Tool for Powder Diffraction, (2017) (Available from:), http://www.cdifx.univ-rennes1.fr/winplotr/winplotr.htm.
[39] A.L. Patterson, Phys. Rev. 56 (1939) 978–982.
[40] D.A. McKeown, P.L. Hagans, L.P.L. Carette, A.E. Russell, K.E. Swider, D.R. Rolison, J. Phys. Chem. B 103 (1999) 4825–4832.
[41] M.A. Vannice, J. Catal. 44 (1976) 152–162.
[42] Z. Kowalczyk, K. Stołecki, W. Raróg-Pilecka, E. Miśkiewicz, E. Wilczkowska, Z. Karpiński, Appl. Catal. A 342 (2008) 35–39.
[43] R. Burch, A.R. Flambard, J. Catal. 78 (1982) 389–405.
[44] W.M.H. Sachtler, M. Ichikawa, J. Phys. Chem. 90 (1986) 4752–4758.